Northumbria Research Link

Northumbria
University
NEWCASTLE

Experimental Verification of LTE Radio Transmissions over Dual-polarization Combined Fibre and FSO Optical Infrastructures

J. BOHATA[1,*], S. ZVANOVEC[1], P.PESEK[1], T. KORINEK[1], M. MANSOUR ABADI[2], AND Z. GHASSEMLOOY [2]

[1]CTU in Prague, Faculty of electrical engineering, Department of electromagnetic fields, Technicka 2, Prague, Czech Republic
[2]Optical Communications Research Group, NCRLab, Faculty of Engineering and Environment, Northumbria University, Newcastle upon Tyne, NE1 8ST, UK
*Corresponding author: bohatja2@fel.cvut.cz

Received XX December 2015; revised XX Month, XXXX; accepted XX Month XXXX; posted XX Month XXXX (Doc. ID XXXXX); published XX Month XXXX

This paper describes the experimental verification of the utilization of long-term evolution (LTE) radio over fibre (RoF) and radio over free space optics (RoFSO) systems using dual-polarization signals for cloud radio access network (C-RAN) applications determining the specific utilization limits. A number of FSO configurations is proposed and investigated under different atmospheric turbulence regimes in order to recommend the best setup configuration. We show that the performance of the proposed link based on the combination of RoF and RoFSO for 64-QAM at 2.6 GHz is more affected by the turbulence based on the measured difference error vector magnitude value of 5.5 %. It is further demonstrated the proposed systems can offer higher noise immunity under particular scenarios with the signal-to-noise ratio reliability limit of 5 dB in the radio frequency domain for RoF and 19.3 dB in the optical domain for combination of RoF and RoFSO links.

OCIS codes: *(060.2605) Free-space optical communications; (060.5625) Radio frequency photonics; (010.1330) Atmospheric turbulence;(060.2310) Fiber optics.*

http://dx.doi.org/10.1364/AO.99.09999

1. INTRODUCTION

The deployment of small cells and the use of higher radio frequency (RF) bands (e.g., millimetre-wave) are two possible options to fulfil the demand for higher data rates in the next generation wireless access networks. The 3rd generation partnership project (3GPP) of long-term evolution (LTE) with low latency, also known as the 4th generation technology supporting high data rates of up to 300 Mbps and 75 Mbps for the down and uplinks respectively, has been proposed and developed [1, 2]. LTE intended for urban areas and operating at a carrier frequency of 2.6 GHz, imposes higher loss in wireless transmission which limits the cell radius because of the degradation of the signal-to-noise ratio (SNR) [3]. In small-cell based systems optical fibres are considered as an ideal backhaul medium to provide sufficient bandwidth, as well as a future-proof capacity upgrade. More recently, the cloud-based radio access networks (C-RAN) technology is being proposed as a cost-effective and power efficient option for deploying small cells to meet the capacity demand of future wireless access networks. C-RAN decouple the digital baseband processing unit (BBU) from the largely analogue remote antenna unit (RAU) and move it to the BBU pool or BBU hotel, thus, allowing the centralized operation of BBUs and a scalable deployment of RAUs as small cells [4]. In such schemes the optical fibre (OF) communications technology plays a significant role when developing network infrastructures, particularly for connections between adjacent cells, RAU and a central unit pool. OF technology covers approximately 35% of the connections between base stations (BS) while the remaining 55% are based on RF wireless technology [5]. This will rise to over 60 % of fibre connected based stations making 4th and upper generations of mobile communications resulting in optical infrastructures becoming the most suitable medium for transportation of radio signals from/to RAUs. The functions of RAUs can be further simplified by transmitting analogue RF signals over OF backhaul networks. Unlike the conventional digital baseband transmission schemes supporting only one service at a time, the radio-over-fibre (RoF) transmission network [6] enables the coexistence of multi-service and multi-operators in a shared resources, thereby offering increased link capacity, advanced networking (i.e., dynamic resources and allocations) and features such as wavelength division multiplexing (WDM)[7] without the need for frequency up-down conversion. Transmission of the LTE signals over OFs was presented in [8] and highlighted improvements of the OF backhaul in terms of power and cost effectiveness. A field trial

demonstration of high capacity optical super-channel transmission, based on optical orthogonal frequency-division multiplexing with hybrid dual-polarization (DP) quadrature amplitude modulation/phase-shift-keying (QAM/QPSK) modulations, was reported in [9] providing up to 21.7 Tb/s transmission capacity over long-haul optical link. Polarization division multiplexing (PDM) of two distinctive orthogonal frequency division multiplexing (OFDM) signals, based on ultra-wide band standards over the RoF system in passive optical networks, was experimentally demonstrated recently in [10] and effectively doubled the capacity of the system. In [11] an experimental investigation of the RoF system over a 100 km of fibre was demonstrated using PDM and the RF frequency bands of 2.6 GHz and 800 MHz with the highest polarization discrimination of ~30 dB.

However, the application of RoF depends on the availability of installed OFs between various network facilities to connect BBU and RAU within the C-RAN architecture and therefore it is possible to considerably extend multiple services over one fibre by using several frequency channels or the WDM technique as showed in [12]. Installation of OF cables can be, especially in urban areas with dense building structures, challenging and costly. Once OF cables are installed, rewiring then becomes a difficult and time-consuming task when the distribution of wireless users (WU) and the number of WUs are changed. Therefore, a limited amount of installed OFs highlights the usefulness of free space optics (FSO) [13] technology as it offers the same features as OFs, but with considerably reduced deployment cost and significantly higher capacity [14] compared to conventional RF wireless approaches.

The concept of radio over FSO (RoFSO) has been experimentally introduced by combining a full optical FSO system (employing a 1 km FSO turbulent link at a wavelength of 1550 nm), together with the digital TV RF signal without any signal conversion in [15, 16]. In [17] a Dense WDM system with RoFSO technology was used to transmit a range of various radio services over a 1 km of FSO link under turbulence conditions offering a similar bandwidth to OF for both indoor and outdoor (short range) applications with the 99.9 % of link availability. Therefore, it is desirable to extend the existing RoF concepts toward RoFSO to cover the entire optical transmission technology within future C-RAN. In such scenarios it is essential to determine system statistics under various channel configurations (i.e., OF, FSO, or a hybrid OF-FSO). A typical scenario employing combined RoF and RoFSO systems is shown in Fig. 1. Among the number of challenges encountered in FSO systems, the atmospheric-induced fading effects (both amplitude and phase) of the received optical signal are the most importance [18]. RoFSO can transmit all types of RF signals without interference, therefore, increasing the number of independent channels, as well as expanding the capacity in the optical domain, becomes highly desirable. WDM based on an optical power allocation scheme, with consideration of the optical modulation index under a total optical transmission power limitation for an adaptive RoFSO link design, was proposed in [19]. A novel wireless network architecture using RoFSO for WLANs, together with the RF assignment mechanism based on RoFSO, was proposed and investigated in [20] offering efficient frequency utilization in terms of both the throughput and fairness index. A coherent multilevel polarization shift keying transceiver using the spatial diversity detection in the FSO channel was theoretically investigated in [21] for different turbulence regimes. The authors reported a predicted power penalty of ~25 dB at a symbol error probability of 10E-8 for the strong turbulence regime (Rytov variance σ_R^2 of 3.5). The first concept of the dual-polarization multiplexing RoFSO system proposed for the LTE radio signal was investigated in [22].

In this paper an optical dual-polarization LTE RoF & RoFSO system for C-RAN networks using the PDM scheme is proposed. Novel experimental results in terms of the measured and simulated error vector magnitude (EVM) statistics are presented and evaluated. We consider four typical channel configurations using combinations

Fig. 1. Example of Radio over fibre and radio over FSO scenario adopting cloud RAN architecture.

of RoF and RoFSO. The performance of RoFSO system is highly influenced by environmental factors, thus, we focus on the FSO channel under the turbulence regime. Based on the investigation of the channel dynamic range and noise immunity tests, we have extended the measurement results to include EVM characteristics and have derived specific limits of utilizations of RoF and RoFSO systems. We show that the performance of the proposed link based on the combination of RoF and RoFSO for 64-QAM at 2.6 GHz is more affected by the turbulence based on the measured difference EVM value of 5.5 %. We further show that the proposed systems can offer higher noise immunity under particular scenarios with the SNR limit of 5 dB in the RF domain for RoF and 19.3 dB in the optical domain for combination of RoF and RoFSO links.

The rest of the paper is structured as follows: section 2 introduces the properties of the proposed system with different configurations and atmospheric turbulence. Results from the measurements and simulations are discussed in section 3, and the conclusions are presented in section 4.

2. EXPERIMENTAL SETUP

A. Main setup description

The experimental setup consists of transmitter (Tx), channel, and receiver (Rx) parts as shown in Fig. 2. On the Tx side both branches are modulated by two independent RF signals prior to the application of a polarization-multiplexing technique for transmitting over the optical channel (OF and FSO).

A distributed feedback (DFB) laser diode (ID-Photnonics TL CoBrite Dx4) at a wavelength of 1550 nm was used as the optical source (OS). The output of OS, passing through a power splitter (PS) (Opneti PBS 15-L-1-1-FA), is externally modulated with two digital RF signals (vector signal generators – R&S SMBV 100 A and SMW 200 A) of the same carrier frequency and equal bandwidth using Mach-Zehnder modulators (MZM) (Thorlabs LN81S). For a detailed description of the influence of MZM on RoF, please refer to [23]. The two orthogonal polarization states of the modulated light beams were controlled using two polarization controllers (PC) and combined via the polarization beam combiner (PBC) prior to being launched into standard SMFs (SSMF). As shown, erbium-doped fibre amplifiers (EDFA) (Keopsys – KPS-BT2-C-10-LN-SA) were used to compensate for the channel loss. Four types of the RoF/RoFSO-based channel configurations were investigated:

i) Setup-A: 5 km of SMF and EDFA
ii) Setup-B: EDFA and the FSO channel
iii) Setup-C: 5 km of SMF, EDFA and the FSO channel
iv) Setup-D: EDFA, 5 km of SMF (representing the typical transmission span for RoF links) and the FSO channel.

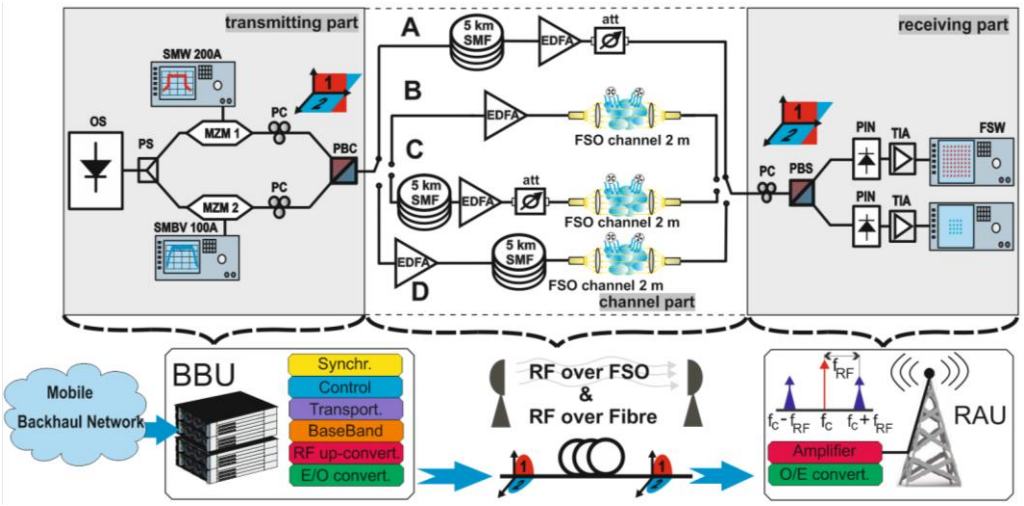

Fig. 2. The schematic diagram of DP-LTE over optical communications for C-RAN architecture (upper part shows laboratory setup; the corresponding network structure is illustrated below).

Since the focus in this work was only on the RoF and RoFSO parts of the RAN system, we did not consider retransmission or signal recovery between OF and FSO parts, which is typically done by the remote RoF units. At the Rx PC was used to adjust the polarization states of the incoming optical signal before being fed into a polarization beam splitter (PBS) according to [10] and [11]. PDM optical signals can be potentially demultiplexed by coherent detection and digital signal processing. Polarization dependence of coherent detection can be then managed by means of optical dynamic polarization control or a polarization diversity Rx [24],[25]. In a conventional polarization diversity Rx, two sets of Rxs are used to independently detect signal components in the two orthogonal polarization states and the original signal is recovered after combining two components, which is rather inefficient in terms of hardware. However, when two PDM channels are simultaneously transmitted at orthogonal polarization states, a polarization diversity Rx in principle can receive both channels, for example, by using optical dynamic polarization control at the Rx. All-optic scheme for PDM systems using dynamic PC has been proposed in [26] It has been suggested that PDM optical signals can potentially be demultiplexed by combining coherent detection and polarization/phase diversity [27].

The Rx is composed of a pair of encapsulated balanced PIN photodiodes (PD) and a transimpedance amplifier (TIA) (Newport 1544-B50). The output of the TIA was captured for further processing using a signal analyzer (R&S FSV). We used LTE evolved universal terrestrial radio access (E-UTRA) test models with 16-QAM and 64-QAM in the polarization state 1 (noted as Pol 1). An independent digital mobile radio service with 16-QAM, having the same parameters (frequency, bandwidth and power) as the signal in Pol 1, was launched to the polarization state 2 (Pol 2).

The polarization orthogonality was continuously verified by monitoring the parameters at the Tx for one polarization state (i.e., Pol 1) while the signal in the second polarization state (i.e., Pol 2) was switched off and on with no influence observed on either the original power magnitude, the SNR, the optical signal to noise ratio (OSNR), or the corresponding EVMs. In the experimental setup we used two commonly adopted LTE frequency bands of 800 MHz and 2.6 GHz with the bandwidth set to 10 MHz. We also set the peak envelope power below the limit of 15 dBm to avoid harmonic distortions at the recovered RF spectrum. All key adopted system parameters are listed in Table I. For the FSO links graded-index lenses (Thorlabs 50-1550A-APC) with an aperture of 1.8 mm and convex lenses with a diameter of 25.4 mm (SMPF_115-APC) were used to launch and couple light from/into the SMF. FSO links were subjected to the atmospheric turbulence in order to assess the performance of the proposed system.

B. Noise conditions

In this section we outline the noise sources associated with the link, in particular the shot noise, thermal noise and relative intensity noise (RIN).

The power of the shot and thermal noise sources can be expressed as the fundamental noise [28]:

$$N_{fund} = (g_{rf} + 1)k_B T\Delta f + \frac{1}{2} q I_{DC} \Delta f R_{out}, \quad (1)$$

where g_{rf} is the RF gain, k_B is Boltzmann's constant, T is the temperature, q is the electronic-charge constant, I_{DC} is the average PD DC current, and R_{out} is the matching load resistance.

Additionally, there is the excess photon noise due to fluctuations of the intensity of the light source as a result of the beating of various spectral components having random phases. For a purely spontaneous source it is given as [29]:

$$\langle \Delta i_{ex}^2 \rangle = \left(\frac{(1+\alpha^2)\langle I \rangle^2 \Delta f}{\Delta \nu_{eff}} \right), \quad (2)$$

where α is the degree of polarization, and $\Delta \nu_{eff}$ is the effective bandwidth. Though all three noise sources can be used to estimate the RIN, it should be noted that $\langle \Delta i_{ex}^2 \rangle$ should only be used for optical sources with a purely spontaneous emission profile.

The RIN, associated with the optical devices, represents the total amount of photon noise per unit bandwidth and is defined as:

$$RIN_{total} = \frac{\langle P_f^2 \rangle}{P^2} = \frac{\langle \Delta i_{th}^2 \rangle + \langle \Delta i_{sh}^2 \rangle}{\langle I \rangle^2 \Delta f} = \frac{4N_{total}}{I_{dc}^2 R_{out}}, \quad (3)$$

where $\langle P_f^2 \rangle$ is the auto-correlated value of the optical power fluctuation at frequency f, which can be measured using an electrical spectrum analyser to represent the total output noise power spectral density N_{total} delivered to R_{out}. P is continuous wave optical power, which contributes to I_{DC}.

Note that the shot noise is divided into two branches (matching circuit and load). With the links employing optical amplifications there are additional noise contributions. The primary noise source in optical amplifiers (e.g., EDFA) adopted in the optical communications is the amplified spontaneous emission (ASE) with a spectrum almost the same as the gain spectrum of the amplifier. When detected, these spontaneously generated photons result in signal-spontaneous (sig-sp) and spontaneous-spontaneous (sp-sp) beat noise currents. The sp-sp beat noise power density is inversely proportional to the $OSNR^2$ whereas the sig-sp beat noise power density is inversely proportional to the OSNR. The sp-sp beat noise also depend on the baseband frequency, with the noise density decreasing with increasing the

baseband frequency. In principle, the sp-sp beat noise intensity spectrum could be as wide as the optical amplifier bandwidth in the absence of optical filtering. From practical point of view the excess noise regime is highly important, where the noise level is higher than the level of shot noise, due to the influence of sig-sp beat noise, etc. Therefore, here we only consider the sig-sp beat noise, which is given as [28]:

$$RIN_{sig-sp} = \frac{4n_{sp}h\nu}{g_{opt}P_{sig}}, \quad (4)$$

where n_{sp} is the spontaneous emission factor, h is Planck´s constant, ν is optical frequency, g_{opt} represents the optical power gain of the EDFA, F_{opt} is the noise factor of the EDFA, and P_{sig} stands for average optical signal power input to the EDFA. Assuming that g_{opt} >>1 the equation (4) can be expressed as:

$$RIN_{sig-sp} \approx \frac{2F_{opt}h\nu}{P_{sig}}. \quad (5)$$

F_{opt} is related to the shot noise and the detection scheme. For an ideal detector $F_{opt} = 2n_{sp}$. The degradation of SNR in RoF and RoFSO links is represented by the RF noise factor F_{rf} with respect to thermally limited input and is defined in terms of the the RoF link output noise power N_{out} as [28]:

$$F_{rf} \equiv \frac{N_{out}}{g_{rf}k_BT}. \quad (6)$$

Typically F_{rf} is enumerated under T = 290 K. We can rewrite the definition of the noise factor by using eq. (3) and the RF gain as:

$$F_{rf} \equiv \frac{V_\pi^2 RIN_{total}}{\pi^2 R_{in}k_BT}, \quad (7)$$

where R_{in} is the input resistance of the MZM and V_π is a convenient parameter to specify the efficiency of an electro-optic intensity modulator, which is defined as the voltage required to change the optical power transfer function from the minimum to the maximum.

In the experimental test setup, the SNR was set in the RF domain directly via the signal generator by including an adding additional noise source while the OSNR was controlled by adding a variable optical attenuator placed directly behind the EDFA in setups A and C to avoid amplifier's gain induced OSNR fluctuations as depicted in fig. 2. In the setup C, we positioned the optical attenuator in front of the optical link to maintain the desired OSNR level over the FSO channel. OSNR was measured using an optical spectrum analyzer (OSA). Here we have adopted the intensity modulation with direct detection (IM/DD) scheme and used single-drive MZMs, which were biased at their maximal transmission point. At the input of the MZM, the field waveform (in time t) can be expressed as [28]:

$$E_{IN}(t) = \kappa\sqrt{2P_{laser}}e^{j\omega_0 t}, \quad (8)$$

where P_{laser} is average laser power at angular frequency ω_0 and κ is a constant relating field and average power. The input voltage to the MZM is defined by:

TABLE 1. SETUP PARAMETERS

Parameter	Value
Carrier frequencies	800 MHz & 2.6 GHz
System bandwidth	10 MHz
OFDM subcarriers	667
OFDM symbols/subframe	7
RF output power	-5 dBm
Modulation scheme	16- and 64-QAM
LTE test models	E-TM2 & E-TM3.2
DFB	
- laser output power	8 dBm
-wavelength	1550 nm
FSO channel length	2 m
FSO channel loss	15 dB
Fibre 5 km loss	1.7 dB
EDFA	
-noise figure	< 5 dB
-return loss	>-40 dB
PIN responsivity	0.75 A/W
TIA bandwidth	10 kHz - 12 GHz

$$V_{IN}(t) = V_{dc} + V_{RF}sin(\omega_0 t), \quad (9)$$

where symbol V_{dc} stands for bias voltage and the expression $V_{RF}sin(\omega_0 t)$ defines the modulating RF signal V_{RF}. Among other factors, IM/DD introduces additive noise to the hybrid radio and photonic system.

C. FSO turbulence effects

There are a number of methods for generating turbulence within an indoor controlled environment including near index matching, liquid filled chambers, spatial light modulators, ion-exchange phase screens, surface etching, and hot air chambers [30]. For assessing the performance of the proposed scheme we have adopted the latter and used an artificial turbulence generator with known, realistic, and repeatable characteristics. Two fans were used to blow hot air into the channel perpendicular to the propagating optical beam. To measure the temperature profile and determine the temperature gradient along the channel, we placed 20 thermal sensors at an interval of 10 cm along the FSO channel. We used Rytov variance and the refractive index structure parameter to characterize strength of the turbulence according to [22]. The variance of the log-intensity signal fluctuation defined by Rytov variance σ_R^2 is given by [31]:

$$\sigma_R^2 = 1.23k^{\frac{7}{6}}C_n^2L^{\frac{11}{6}}, \quad (10)$$

where k = 2π/λ is the wavenumber and λ is the transmission wavelength.

C_n^2 is the refractive index structure parameter (the main measure of the turbulence scale), which is given as [18]:

$$C_n^2 = (79 \times 10^{-6}\frac{P_a}{T^2})^2C_T^2, \quad (11)$$

where P_a is the atmospheric pressure in millibars. C_T^2 is the temperature structure constant, which is defined as [18]:

$$C_T^2 = (T_1 - T_2)^2/L_p^{2/3}). \quad (12)$$

T_1 and T_2 are temperatures at two points separated by distance L_p. Knowing the thermal distribution along the FSO propagation path, it is possible to determine C_T^2 and then C_n^2.

3. EXPERIMENTAL AND SIMULATION RESULTS

The experimental section is divided into three parts. In part A the transmission properties of four selected scenarios (setups A, B, C and D; see Fig. 2) were tested under the steady-state condition with no turbulence. Part B describes the detailed investigation of the dynamic range and noise conditions of the RoF system compared to the hybrid RoF and RoFSO (setups A and C) systems. Finally, part C outlines the comparison of the links including the FSO channel under turbulence regimes (setups B, C and D).

A. System properties

We have tested the suitability of proposed scenarios A, B, C, and D using the polarization multiplexed technique for RF signals. Two standardized E-UTRA test models were selected for the investigation of the channel quality: E-UTRA Test model 2 and E-UTRA Test model 3.2 [32]. Both test models are specified for testing E-UTRA systems with an emphasis on either the dynamic range or the quality of the transmitted signal using 64- and 16-QAM, respectively.

Scenarios A and B evinced EVM around 1 % meanwhile scenarios C and D evinced EVM between 2 % and 3%. It can be observed scenarios A and B offer roughly two or three times better EVM performance when compared to the hybrid RoF and RoFSO systems (C and D). Nevertheless, all scenarios show EVM values dramatically below the maximal 3GPP LTE EVM threshold of 8 % recommended for high data rate systems [33]. Note that for the setup A, with 5 km of SMF, the output power of EDFA had to be decreased in order to ensure that the PIN PD was not saturated or damaged. The gain of the EDFA was preserved throughout the experimental work in order to maintain similar conditions. Last but not least, we simulated the

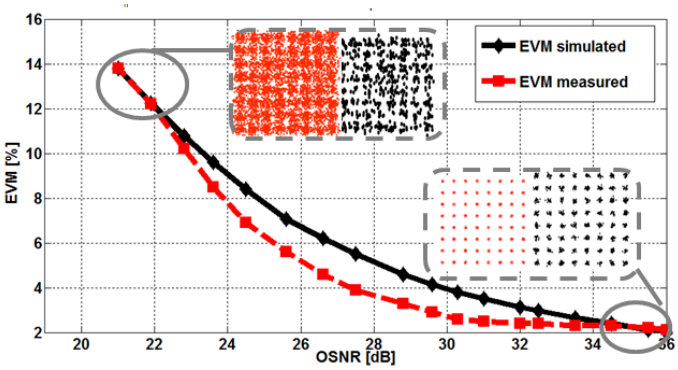

Fig. 3. Simulated and measured EVM as a function of OSNR for 64-QAM at a frequency of 2.6 GHz for 5 km of SMF (setup A). Inset shows the constellation diagrams

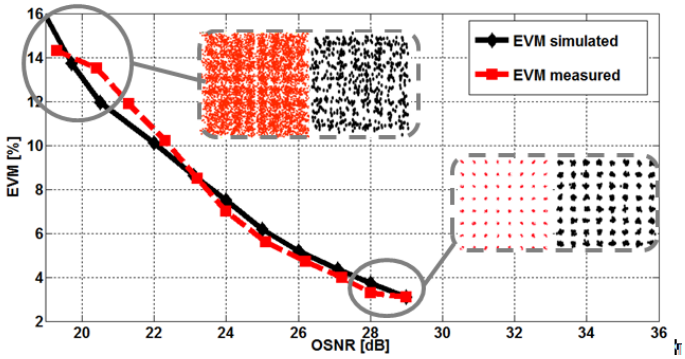

Fig. 4. Simulated and measured EVM as a function of OSNR for 64-QAM at a frequency of 2.6 GHz for 5 km of SMF + FSO channel (setup C). Inset shows the constellation diagrams.

conditions of a real system by employing an EDFA in order to further increase the transmission span.

B. Noise parameters

Next we carried out several tests focusing on the quality of the E-UTRA signals transmitted over the optical channels for a range of OSNR and SNR values. These tests were focused on the hazard noise effects described in Section 2B, which can significantly reduce both OSNR and SNR, thus degrading the performance of RoF and RoFSO systems. At first, we carried out simulations for the EVMs for the proposed system featuring SMF and FSO sections (setups A and C). Subsequent measurements using a frequency of 2.6 GHz and 64-QAM were also carried out to validate the simulated results. The constellation diagrams of the 64-QAM and the evolution of the EVM parameter were evaluated both experimentally and by mean of simulation, which was then correlated. Figures 3 and 4 depict the predicted and measured EVM as a function of the OSNR for setups A and C, respectively. For the setup A, there is a mismatch between the measured and predicted EVMs, with the maximum difference

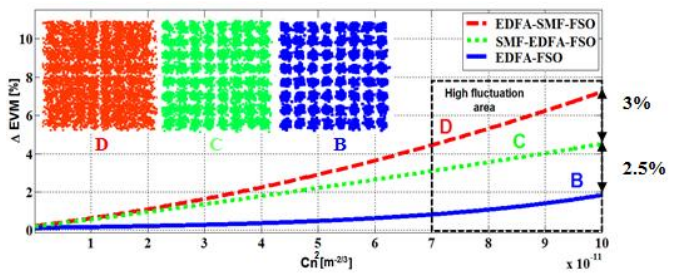

Fig. 6. ΔEVM as a function of the refractive index structure parameter C_n^2 for setups B, C and D for 64-QAM at 2.6 GHz and OSNR corresponding to maximal values for each particular scenario.

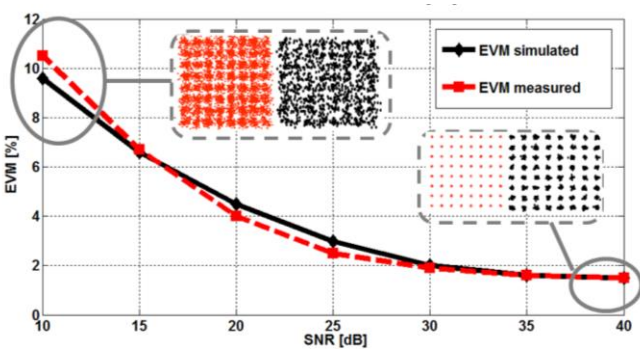

Fig. 5. Simulated and measured EVM as a function of SNR for 64-QAM at a frequency of 2.6 GHz for 5 km of SMF (setup C). Insets show the constellation diagrams

of < 2 % at an OSNR of 28 dB. This is, in all probability, caused by the slightly different properties of simulated and real behavior of EDFAs, which are due to ASE as being the main noise source in the optical domain. For the setup C, there is a good match between the measured and predicted plots. The measured (red) and simulated (black) constellation diagrams are also shown in Figs. 3 and 4. These plots show that the RoF with a 5 km of fibre can operate over a wide range of OSNR (i.e., from 36 to 21 dB), whereas for the hybrid RoF and RoFSO links the OSNR range is only 10 dB (from 29 to 19.3 dB). In the case of the FSO channel, this can be attributed to the power budget being significantly lower and the noise floor belonging to a particular scenario. The experimental and simulated EVM curves for the setup C show the same trend for OSNR values of 29 dB and 21 dB as in the setup A with the only difference being the initial EVM values. In addition, as described above, the EDFA power had to be reduced while using the setup A, which resulted in a minimal OSNR value of ~21 dB. It can be observed that the proposed systems even operate over the recommended 8 % EVM limit when using 64-QAM, but at the cost of higher error probability.

Next we investigated the EVM as a function of the SNR, which was measured on the Rx side, for the setup C for 64-QAM at a frequency of 2.6 GHz with no turbulence as shown in Fig. 5. The insets illustrate the corresponding constellation diagrams. The plots demonstrate a good agreement between the measured and simulated results. The SNR dynamic range show a decrease of ~5 dB compared to the setup A (while employing only a 5 km of SMF). Both scenarios meet dynamic range requirements for home, local and wide area BSs specified by [32].

C. Turbulence

Finally, we compared the performance of both RoFSO (setup B) and the hybrid RoF and RoFSO (setups C and D) systems under the influence of atmospheric turbulence. The average values of ΔEVM for these particular scenarios were captured for a range of the refractive index structure parameter C_n^2. Since the initial magnitude of EVM was different for particular scenarios, all EVM values were aligned by showing the ΔEVM. We have adopted the frequency of 2.6 GHz for further detailed investigations since the performance of the systems for 800 MHz and 2.6 GHz are almost the same. We compare all optical-based systems including the FSO part (Setups B, C and D from Fig. 2) at 2.6 GHz for 64-QAM for different turbulence regimes in terms of changes in EVM, as illustrated in Fig. 6.

The higher is C_n^2 the larger is the fluctuation of the power magnitude and its corresponding EVM values, which can exceed the reliability limits of the RAN system. The proposed LTE test model for 64-QAM fulfills the reliability and the high data rate limit of EVM (i.e., < 8 %). Results indicate a RoFSO scenario evinces the best properties comparable to the hybrid RoF and RoFSO setups C and D where tolerable limits were exceeded approximately beyond the threshold C_n^2 of ~7.0E-11 $m^{-2/3}$, in particular because of high fluctuations observed in EVM. In other words, the use of the RoF technology,

together with RoFSO under the turbulence condition, resulted in slightly reduced performance compared with the RoFSO link in terms of increased mean value of ΔEVM by 2.5 % and 5.5 % in the setups C and D, respectively at C_n^2 of ~ 1E-10 $m^{-2/3}$. This cannot be attributed only to added SMF (with an average EVM of 1 %), and therefore the overall system EVM has to be determined. The hybrid setups (C and D) offers a reliable high data rate transmission for the C_n^2 value up to ~7E-11 $m^{-2/3}$, which corresponds to C_n^2 of 5.37E-14 $m^{-2/3}$ in the case of a 100 m long FSO link, extrapolated through Rytov variance expression (11). The predicted values largely fall into the moderate turbulence regime, thus representing a typical maximal turbulence strength according to [18] and [34] where a 1 km long FSO link under a real turbulence condition was investigated. By placing the EDFA between the RoF and RoFSO systems, to compensate for the loss in the RoF link and boost the incoming signal prior to RoFSO link, the EVM is improved by ~3 %, as shown within the high fluctuation region in Fig. 6. Note that the optical output power (OS and EDFA) levels were kept at a relatively low level to avoid the more significant role of nonlinear effects in OF.

4. CONCLUSION

Having proposed an optical dual-polarization LTE RoF & RoFSO system for C-RAN networks and having evaluated its performance in terms of the measured and simulated EVM statistics, we showed the configuration of radio systems for 64-QAM at 2.6 GHz, incorporating FSO under the turbulence regimes, which lead to EVM values below 8 % for C_n^2 of up to 5.37E-14 $m^{-2/3}$ when considering a 100 m long FSO link. We also showed that the performance of the proposed link based on the combination of RoF and RoFSO was more affected by the turbulence with the measured ΔEVM value increased to 5.5 %. However, the EVM was reduced by ~3 % when placing EDFA between RoF and RoFSO links. The proposed systems can offer higher noise immunity under particular scenarios with the SNR reliability limits of 5 dB in the RF domain for RoF and 19.3 dB in the optical domain for RoFSO links. There were no significant changes in the polarization of the radio PDM system while propagating through the fibre and FSO channels, thus illustrating proposed system attributes to a higher transmission capacity. The employment of the dual-polarization solutions, as part of the C-RAN infrastructures, creates a dense network between the RF base-end parts and central cloud pools, thus making the infrastructure simpler and more robust. Moreover, the proposed technique can be adopted for other radio services such as WiFi or Wimax, thus leading to improved network convergence.

Funding Information. SGS14/190/OHK3/3T/13; EU COST Action OPTICWISE (IC 1101)

ACKOWLEDGMENT. Authors would like to thank Rohde & Schwarz – Praha, s.r.o. for the technical support.

References

1. S. Seung-Chul and L. Young-Poong, "Testing of early applied LTE-Advanced technologies on current LTE service to overcome real network problem and to increase data capacity," in Proceedings of Advanced Communication Technology, (IEEE, 2013), pp. 275-281.
2. S. Kanchi, et al., "Overview of LTE-A technology," in Proceedings of IEEE Global High Tech Congress on Electronic (IEEE, 2013), pp. 195-200.
3. T. Wirth,. V. Venkatkumar, T. Haustein, E. Schulz, "LTE-Advanced Relaying for Outdoor Range Extension," in Proceedings of Vehicular Technology Conference Fall, (IEEE, 2009), pp. 1-4.
4. A. Checko, H. L. Christiansen, Y. Yan, L. Scolari, G. Kardaras, M. S. Bertger and L. Dittman, " Cloud RAN for Mobile Networks-A Technology Overview," Commun. Surveys Tuts, vol. **17**, 405-426 (2015).
5. J. Segel, "lightRadio Portfolio: White Paper 3," Alcatel-Lucent Bell Labs, Tech. Rep., 2011.
6. S. Ting, J. Zheng, J. Wang, M. Zhu, Z. Dong, M. Xu, M. Zhang, X. Chen and G. K. Chang, "Multiservice Wireless Transport Over RoF Link With Colorless BS Using PolM-to-IM Convertor," Photon. Technol. Lett., vol. 27, 403-406 (2015).
7. H. Al-Raweshidy and S. Komaki, Radio Over Fiber Technologies for Mobile Communications Networks (Artech House, 2002).
8. S. Aleksic, M. Deruyck, W. Joseph, "Energy efficiency of optically backhauled LTE: A case study," in Proceedings of Electromagnetics in Advanced Applications, (IEEE, 2013), pp. 390-393.
9. H. Y. Huang,M. F. huang, E. Ip, E. Mateo, P. N. Ji, D. Qian, A. Tanaka, Y. Shao, T. Wang, Y. Aono, T. Tajima, T. J. Xia and G. A. Wellbrock, "High-Capacity Fiber Field Trial Using Terabit/s All-Optical OFDM Superchannels With DP-QPSK and DP-8QAM/DP-QPSK Modulation," J.Lightwave Technol., vol. **31**, pp. 546-553, (2013).
10. M. Morant, J. Perez and R. Llorente, "Polarization Division Multiplexing of OFDM Radio-over-Fiber Signals in Passive Optical Networks," Advances in Opt. Tech., vol. **9** (2014).
11. M. Morant, J. Prat and R. llorente, "Radio-Over-Fiber Optical Polarization-Multiplexed Networks for 3GPP Wireless Carrier-Aggregated MIMO Provision," J.Lightwave Technol., vol. **32**, 3721-3727 (2014).
12. C. Liu, L. Zhang, M. Zhu, J. Wang, L. Cheng and G. K. Chang "A Novel Multi-Service Small-Cell Cloud Radio Access Network for Mobile Backhaul and Computing Based on Radio-Over-Fiber Technologies," J.Lightwave Technol., vol. **31**, 2869-2875 (2013).
13. Z. Ghassemlooy, W. Popoola and S.Rajbhandari, Optical Wireless Communications: System and Channel Modelling with MATLAB® (Taylor & Francis, 2012).
14. G. Parca, A. Shahpari, V. Carrozzo, G. M. Beleffi and A. L. J. Teixeira, "Optical wireless transmission at 1.6-Tbit/s (16×100 Gbit/s) for next-generation convergent urban infrastructures," Opt. Eng., vol. **52**, 116102-116102 (2013).
15. C. Ben Naila, K. Wakamori, M. Matsumoto and K. Tsukamoto, "Transmission analysis of digital TV signals over a radio-on-FSO channel," in Proceedings of ITU Kaleidoscope 2011: The Fully Networked Human? - Innovations for Future Networks and Services (ITU, 2011), pp. 1-7.
16. C. B. Naila, K. Wakamori and M. Matsumoto, "Transmission analysis of digital TV signals over a Radio-on-FSO channel," IEEE Commun. Mag., vol. **50**, 137-144 (2012).
17. D. Pham Tien, A. M. Shah, K. Kazaura, K. Wakamori "A study on transmission of RF signals over a turbulent free space optical link," in Proceedings of Microwave photonics, 2008, jointly held with the 2008 asia-pacific microwave photonics conference, (IEEE, 2008), pp. 173-176.
18. L. C. Andrews and R. L. Phillips, Laser beam propagation through random media (SPIE Press, 2005).
19. K. Kyung-Hwan, T. Higashino, K. Tsukamoto, S. Komaki, "WDM optical power allocation method for adaptive radio on free space optics system design," in Proceedings of Microwave Photonics, 2011 International Topical Meeting on & Microwave Photonics Conference, (IEEE, 2011), pp. 361-364.
20. P. Yue, X. Yi, Z. Li , "Research on Radio Frequency Assignment Mechanism of the Distributed Antenna System Based on Radio over Free Space Optics Technology," in Proceedings of IEEE Services Computing Conference, (IEEE, 2010), pp. 526-530.
21. X. Tang, Z. Ghassemlooy, S. Rajbhandari, W. O. Popoola and C. G. Lee, "Coherent Heterodyne Multilevel Polarization Shift Keying With Spatial Diversity in a Free-Space Optical Turbulence Channel," J.Lightwave Technol., vol. **30**, 2689-2695 (2012).
22. J. Bohata, S. Zvanovec, T. Korinek, M. A. Abadi and Z. Ghassemlooy, "Characterization of dual-polarization LTE radio over a free-space optical turbulence channel," Appl. Optics, vol. **54**, 7082-7087, 2015/08/10 (2015).
23. T. Kanesan, W. Pang Ng, Z. Ghassemlooy and C. Lu, "Investigation of Optical Modulators in Optimized Nonlinear Compensated LTE RoF System," J.Lightwave Technol., vol. **32**, 1944-1950 (2014).
24. B. Glance, "Polarization independent coherent optical receiver," J. Lightwave Technol., vol. **5**, p.p. 274–276 (1987)

25. Yan Han and Guifang Li, "Coherent optical communication using polarization multiple-input-multiple-output," Opt. Express, vol **13**, p.p. 7527-7534 (2005)
26. X. Steve Yao, L.-S. Yan, B. Zhang, A.E. Willner and J. Jiang, "All-optic scheme for automatic polarization division demultiplexing," Opt. Express, vol. **15**, pp. 7407-7414 (2007).
27. M. G. Taylor, "Coherent detection method using DSP for demodulation of signal and subsequent equalization of propagation impairments," IEEE Photon. Technol. Lett. , vol. **16**, p.p. 674–676 (2004)
28. C. H. Lee, Microwave Photonics, Second Edition (Taylor & Francis, 2013).
29. Y. Wang, I. Tomov, J. S. Nelson, Z. Chen, H. Lim and F. Wise, "Low-noise broadband light generation from optical fibers for use in high-resolution optical coherence tomography," J. Opt. Soc. Am., vol. **22**, 1492-1499, 2005/08/01 (2005).
30. R. Rampy, D. Gavel, D. Dillon and S. Thomas, "Production of phase screens for simulation of atmospheric turbulence," Appl. Optics, vol. **51**, 8769-8778, 2012/12/20 (2012).
31. R. L. Fante, "Electromagnetic beam propagation in turbulent media," Proc. IEEE, vol. **63**, 1669-1692 (1975).
32. The 3rd Generation Partnership Project. Available: http://www.3gpp.org/
33. B. Bangerter, S. Talwar, R. Arefi and K. Stewart, "Networks and devices for the 5G era," IEEE Commun. Mag., IEEE, vol. **52**, 90-96 (2014).
34. C. B. Naila, A. Bekkali, K. Wakamori and M. Matsumoto, "Performance Analysis of CDMA-Based Wireless Services Transmission Over a Turbulent RF-on-FSO Channel," J. Opt. Commun. Netw., vol. **3**, 475-486, 2011.